


RESEARCH PAPER



Compound heterozygous *CACNA1H* mutations associated with severe congenital amyotrophy

Melissa T. Carter ^a, Hugh J. McMillan^a, Andriy Tomin ^b, and Norbert Weiss ^b

^aChildren's Hospital of Eastern Ontario Research Institute, University of Ottawa, Ottawa, Ontario, Canada; ^bInstitute of Organic Chemistry and Biochemistry, Czech Academy of Sciences, Prague, Czech Republic

ABSTRACT

Neuromuscular disorders encompass a wide range of conditions often associated with a genetic component. In the present study, we report a patient with severe infantile-onset amyotrophy in whom two compound heterozygous variants in the gene *CACNA1H* encoding for Ca_v3.2 T-type calcium channels were identified. Functional analysis of Ca_v3.2 variants revealed several alterations of the gating properties of the channel that were in general consistent with a loss-of-channel function. Taken together, these findings suggest that severe congenital amyotrophy may be related to *CACNA1H* and would represent a new phenotype associated with mutations in this gene.

ARTICLE HISTORY

Received 24 April 2019
Revised 26 April 2019
Accepted 26 April 2019

KEYWORDS

Congenital amyotrophy;
CACNA1H; mutations;
calcium channel; Ca_v3.2
channel; T-type channel

Introduction

Neuromuscular disorders (NMD) encompass a wide range of conditions including amyotrophic lateral sclerosis (ALS), congenital muscular dystrophies and myopathies, Duchenne muscular dystrophy, and spinal muscular atrophy. They are characterized by progressive muscle degeneration and weakness that primarily or secondarily impair skeletal muscles and their innervation. The onset of NMD ranges from *in utero* to old age, but primarily affect infants, children, and teenagers [1]. Although some NMD are acquired, the vast majority are genetic, and may display autosomal recessive, autosomal dominant, or X-linked inheritance [2]. It is also apparent that NMD phenotypes may vary widely even in individuals carrying the same disease-causing mutation, suggesting the existence of additional factors such as modifier genes that contribute to the onset, severity, and duration of the disease [3].

Recently, whole exome sequence analysis has identified two compound heterozygous recessive missense mutations in the gene *CACNA1H* in a patient with ALS [4,5]. *CACNA1H* encodes for Ca_v3.2 channel, a member of the voltage-gated calcium channel family [6]. Ca_v3.2 channels are widely expressed throughout the body including the central and peripheral nervous system, heart, kidney, smooth muscle, as well as in

several neuroendocrine organs [7]. Through their ability to support low-threshold calcium influx (T-type current), they serve essential physiological processes including neuronal firing, hormone secretion, smooth muscle contraction, and myoblast fusion [8]. Their physiological implication is further exemplified by the existence of polymorphisms in *CACNA1H* associated with a number of human disorders including several forms of epilepsy [9], autism spectrum disorders [10,11], congenital pain [12], primary aldosteronism [13,14], and ALS [4,5].

In the present study, we report a patient with severe congenital amyotrophy in whom two compound heterozygous variants in *CACNA1H* were identified. Functional analysis of Ca_v3.2 variants revealed altered channel gating, strengthening the genetic association of *CACNA1H* with NMD.

Materials and methods

Whole exome sequencing

Whole exome sequencing was performed at a commercial laboratory (GeneDx). Using genomic DNA from the proband and both parents, exonic regions and flanking splice junctions were selected, sequenced, and analyzed as per established proprietary protocols using an Illumina

sequencing system with 100 bp or greater paired end reads. Reads were aligned to human genome build GRCh37/UCSC hg19 and analyzed for sequence variants using a custom-developed analysis tool (Xome Analyzer). Mean depth of coverage was 100x.

Plasmid cDNA constructs

The human wild-type $Ca_v3.2$ in pcDNA3.1 [15] was used as template to introduce separately the V681L and D1233H mutations by site-directed mutagenesis using the Q5[®] Site-Directed Mutagenesis Kit (NEB) and the following pairs of primers: p.V681L: 5'-GGGCCTCAGTttgCCCTGCC-3' (forward) and 5'-GACAGATGGCCAGGGCC-3' (reverse); p.D1233H: 5'-CCTGCGCATCcacAGCCACCG-3' (forward) and 5'-AAG AAGTCGCTGGGCAGG-3' (reverse). Final constructs were verified by sequencing.

Cell culture and heterologous expression

Human embryonic kidney tsA-201 cells were grown in DMEM medium supplemented with 10% fetal bovine serum and 1% penicillin/streptomycin (all media purchased from Invitrogen) and maintained under standard conditions at 37°C in a humidified atmosphere containing 5% CO₂. Heterologous expression of $Ca_v3.2$ channels was performed by transfecting cells with plasmid cDNAs encoding for $Ca_v3.2$ channel variants using the calcium/phosphate method as previously described [16].

Recording of T-type currents

Patch clamp recording of T-type currents in tsA-201 cells expressing $Ca_v3.2$ channels was performed 72 h after transfection in the whole-cell configuration at room temperature (22–24°C). The bath solution contained (in millimolar): 5 BaCl₂, 5 KCl, 1 MgCl₂, 128 NaCl, 10 TEA-Cl, 10 D-glucose, 10 4-(2-hydroxyethyl)-1-piperazineethanesulfonic acid (HEPES) (pH 7.2 with NaOH). Patch pipettes were filled with a solution containing (in millimolar): 110 CsCl, 3 Mg-ATP, 0.5 Na-GTP, 2.5 gCl₂, 5 D-glucose, 10 EGTA, and 10 HEPES (pH 7.4 with CsOH), and had a resistance of 2–4 MΩ. Recordings were

performed using an Axopatch 200B amplifier (Axon Instruments) and acquisition and analysis were performed using pClamp 10 and Clampfit 10 software, respectively (Axon Instruments). The linear leak component of the current was corrected online, and current traces were digitized at 10 kHz and filtered at 2 kHz. The voltage dependence of activation of $Ca_v3.2$ channels was determined by measuring the peak T-type current amplitude in response to 150 ms depolarizing steps to various potentials applied every 10 s from a holding membrane potential of –100 mV. The current-voltage relationship (I/V) curve was fitted with the following modified Boltzmann Equation (1):

$$I(V) = G_{max} \frac{(V - V_{rev})}{1 + \exp\left(\frac{V_{0.5} - V}{k}\right)} \quad (1)$$

with $I(V)$ being the peak current amplitude at the command potential V , G_{max} the maximum conductance, V_{rev} the reversal potential, $V_{0.5}$ the half-activation potential, and k the slope factor. The voltage dependence of the whole-cell Ba²⁺ conductance was calculated using the following modified Boltzmann Equation (2):

$$G(V) = \frac{G_{max}}{1 + \exp\left(\frac{V_{0.5} - V}{k}\right)} \quad (2)$$

with $G(V)$ being the Ba²⁺ conductance at the command potential V .

The voltage dependence of the steady-state inactivation of $Ca_v3.2$ channels was determined by measuring the peak T-type current amplitude in response to a 150 ms depolarizing step to –20 mV applied after a 5 s-long conditioning prepulse ranging from –120 mV to –30 mV. The current amplitude obtained during each test pulse was normalized to the maximal current amplitude and plotted as a function of the prepulse potential. The voltage dependence of the steady-state inactivation was fitted with the following two-state Boltzmann function (3):

$$I(V) = \frac{I_{max}}{1 + \exp\left(\frac{V - V_{0.5}}{k}\right)} \quad (3)$$

with I_{max} corresponding to the maximal peak current amplitude and $V_{0.5}$ to the half-inactivation voltage.

The recovery from inactivation was assessed using a double-pulse protocol from a holding

potential of -100 mV. The cell membrane was depolarized for 2 s at 0 mV (inactivating prepulse) to ensure complete inactivation of the channel, and then to -20 mV for 150 ms (test pulse) after an increasing time period (interpulse) ranging between 0.1 ms and 2 s at -100 mV. The peak current from the test pulse was plotted as a ratio of the maximum prepulse current versus interpulse interval. The data were fitted with the following single-exponential function (4):

$$\frac{I}{I_{max}} = A \times \left(1 - \exp \frac{-t}{\tau} \right) \quad (4)$$

where τ the time constant of channel recovery from inactivation.

Statistical analysis

Values are presented as mean \pm S.E.M. for n experiments. Statistical significance was determined using a one-way ANOVA test followed by Dunnett multiple comparison test. * $p < 0.05$, ** $p < 0.005$, *** $p < 0.001$.

Results

Clinical characteristics and genetic analysis

The patient is a 13-month-old girl who was born at term following a pregnancy complicated by severe polyhydramnios treated with amnioreduction at 31 weeks. Her birth weight was 2.9 kg (20% ile). Her Apgar score (Appearance, Pulse, Grimace, Activity, and Respiration) used to summarize the health of newborn children was critically low (2 at 1-min and 5-min) and was intubated for poor respiratory effort, absent gag and suck. She had arthrogryposis, areflexia, and no antigravity movements. Nerve conduction studies showed intact sensory but absent motor responses. Magnetic resonance imaging (MRI) of her brain was unremarkable. However, the MRI of her muscles noted severe and diffuse amyoplasia with largest muscles being right biceps femoris (8 x 5 mm at widest diameter) and medial gastrocnemius (8 x 3 mm) (Figure 1(a,b)). A biopsy of the vastus lateralis revealed no viable muscle and repeat biopsies of the gastrocnemius noted a strong predominance of type 1 fibers and a marked variability of fiber size.

She remains fully ventilated via tracheostomy with no antigravity movement at 13 months old. Whole exome sequencing identified two compound heterozygous variants (c.2041G>T and c.3697G>C) in *CACNA1H*, causing the substitution of the valine (V) 681 by a leucine (L) (p.V681L) and of the aspartic acid (D) 1233 by a histidine (H) (p.D1233H) in the $Ca_v3.2$ T-type calcium channel, respectively. These mutations were inherited from the father and mother, respectively, who have no symptoms of muscle disease (Figure 1(c)). The p.V681L and p.D1233H mutations are located within the intracellular loops connecting domains I-II and domains II-III of $Ca_v3.2$ channel, respectively (Figure 1(d)).

Expression of $Ca_v3.2$ channel variants

To assess the functional consequence of *CACNA1H* variants, the two mutations were introduced separately into the human $Ca_v3.2$ channel, and functional expression was assessed by patch clamp recording of T-type currents in tsA-201 cells expressing $Ca_v3.2$ channel variants. Cells expressing WT, V681L and D1233H $Ca_v3.2$ channel variants, or co-expressing the two-channel variants (V681L + D1233H) to resemble the heterozygous status of the patient for the two mutations, displayed characteristic low-threshold voltage-activated T-type currents (Figure 2(a,b)). The maximal T-type conductance in cells expressing $Ca_v3.2$ variants was similar (V681L: 756 ± 49 pS/pF, $n = 45$; D1233H: 640 ± 60 pS/pF, $n = 48$) and was not significantly different from cells expressing the WT channel (688 ± 59 , $n = 45$) (Figure 2(c,d)) and Table (1)).

These results indicate that the V681L and D1233H mutations do not alter the expression level of $Ca_v3.2$ channels.

Gating properties of $Ca_v3.2$ channel variants

To assess the functional properties of $Ca_v3.2$ variants, we analyzed the voltage-dependence of T-type current activation in cells expressing WT, V681L, D1233H, or co-expressing the V681L and D1233H channel variants (co-expression of the two separate cDNA constructs each carrying one mutation). The mean half-activation potential in cells expressing the

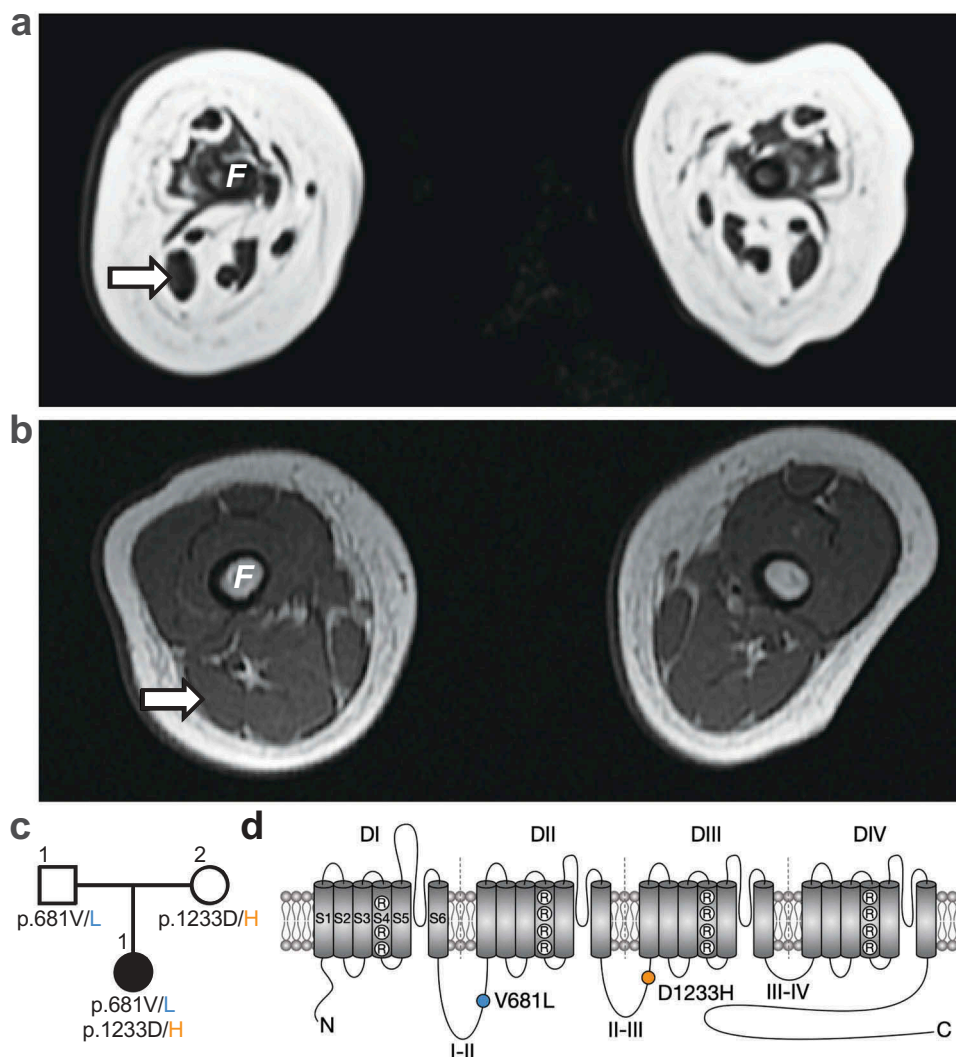


Figure 1. Whole exome sequencing identifies two *CACNA1H* missense mutations associated with severe congenital amyotrophy. (a) Whole-body magnetic resonance T1 weighted images (T1WI) 3T (axial view) of the thigh at 6 weeks old revealed severe muscle amyotrophy. No muscle was visualized in the anterior compartment. Her right biceps femoris (arrow) measured 8×5 mm at its widest. (b) For comparison, a T1WI (axial view) from a hypotonic boy with nemaline myopathy was performed at 4 months old. His biceps femoris measured 14×9 mm. F: femur. (c) Family pedigree chart. Filled and open symbols indicate affected and unaffected individuals, respectively. (d) Location of the p.V681L (blue circle) and p.D1233H mutations (orange circle) within the secondary membrane topology of Ca_v3.2 channel.

V681L variant was shifted by 3.5 mV ($p = 0.0039$) toward hyperpolarized potentials (-43.4 ± 0.9 mV, $n = 45$) compared to cells expressing the WT channel (-39.9 ± 0.6 mV, $n = 45$) (Figure 3(a,b) and Table (1)). Although the mean half-activation potential of T-type currents measured in cells expressing the D1233H variant was not significantly altered, we observed a significant decrease ($p = 0.0429$) of the inactivation slope factor (5.0 ± 0.2 , $n = 48$) compared to WT channels (5.6 ± 0.2 , $n = 45$) (Figure 3(c) and Table (1)). To further investigate the gating properties of Ca_v3.2 variants, we assessed the

voltage-dependence of the steady-state inactivation of the T-type current. We observed a hyperpolarized shift of the mean half-inactivation potential by 5.5 mV ($p < 0.0001$) in cells expressing the V681L variant alone (-75.3 ± 1.2 mV, $n = 30$) and by 4.2 mV ($p = 0.0027$) in cells co-expressing the V681L and D1233H variants (-74.0 ± 1.0 mV, $n = 31$) compared to cells expressing the WT channel (-69.8 ± 0.6 mV, $n = 32$) (Figure 3(d-f) and Table (1)). In contrast, the voltage-dependence of steady-state inactivation of the T-type current in cells expressing the D1233H remained unaltered (Figure 3(d-f) and Table (1)). In addition,

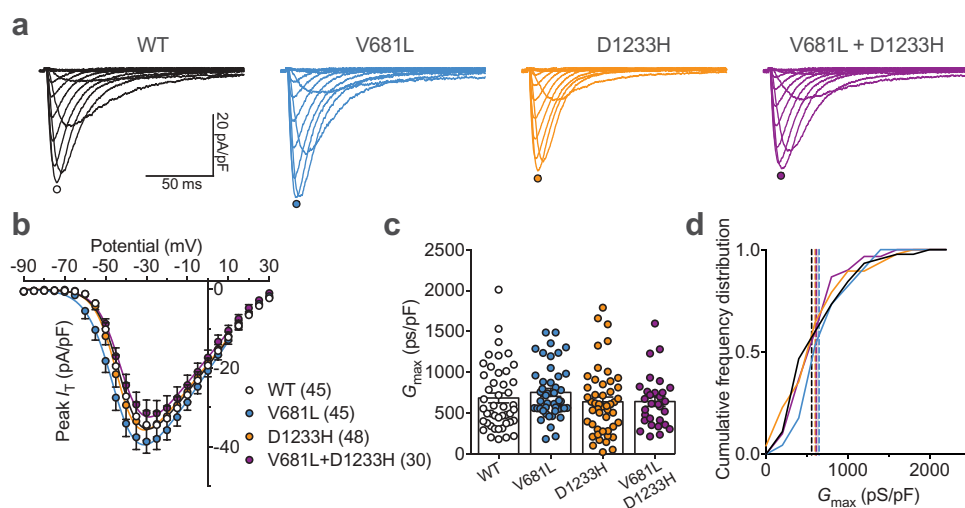


Figure 2. Functional expression of $\text{Ca}_v3.2$ variants. (a) Representative T-type current traces recorded from cells expressing WT (black traces), V681L (blue traces), D1233H (orange traces), and co-expressing V681L and D1233H channel variants (purple traces) in response to 150 ms depolarizing steps ranging between -90 mV and 30 mV from a holding potential of -100 mV. (b) Corresponding mean peak current-voltage (I/V) relationship. (c) Corresponding mean maximal macroscopic conductance (G_{max}) values obtained from the fit of the I/V curves with the modified Boltzmann Equation (1). (d) Cumulative frequency plot of data shown in (C). Dotted lines indicate the median values for each distribution (WT: 558 pS/pF; V681L: 648 pS/pF; D1233H: 601 pS/pF; V681L + D1233H: 615 pS/pF).

recovery from inactivation (Figure 3(g,h) and Table (1)) as well as inactivation and inactivation kinetics remain similar between the channel variants, and only a mild acceleration of the inactivation kinetic of the V681L variant (18.4 ± 0.9 , $n = 30$) was observed compared to the WT channel (21.9 ± 1.0 , $n = 45$) (Figure 3(i) and Table (1)).

Collectively, these data indicate that the V681L and D1233H mutations produce mild but significant alterations of the gating of $\text{Ca}_v3.2$ by altering the voltage dependence of activation and inactivation of the channel.

Window current of $\text{Ca}_v3.2$ channel variants

Considering the effect of the V681L and D1233H mutations on the voltage dependence of activation and inactivation of $\text{Ca}_v3.2$ channels, we analyzed the window current of $\text{Ca}_v3.2$ variants as the area under the overlap between the activation and inactivation curves (Figure 4(a)). We observed a decrease of the window current generated by $\text{Ca}_v3.2$ variants. For instance, the mean area of the window current was decreased by 22% ($p = 0.0055$) and 19% ($p = 0.0188$) in cells expressing the V681L and D1233H variants, respectively (Figure 4(b,c)). Consistent with this observation, the window

current in cells co-expressing the V681L and D1233H channel variants were decreased by 22% ($p = 0.0079$) compared to cells expressing the WT channel (Figure 4(b,c)). In addition, we observed a hyperpolarized shift of the peak-voltage of the window current by 4.6 mV ($p < 0.0001$) in cells expressing the V681L variant (Figure 4(d)).

Altogether, these data indicate that alteration of the voltage-dependence of activation and inactivation caused by the V681L and D1233H mutations ultimately translates into a decrease of the window current supported by $\text{Ca}_v3.2$ variants.

Discussion

Here we describe two compounds heterozygous *CACNA1H* mutations identified in a case-unaffected-parents trio with infantile-onset NMD. The two mutations, V681L and D1233H, are located within the intracellular loops connecting domains I and II (I-II loop) and II and III (II-III loop) of the $\text{Ca}_v3.2$ T-type calcium channel. Previous structure-function studies have documented the role of the I-II loop of $\text{Ca}_v3.2$ in the control of the gating and surface expression of the channel [17,18]. Additionally, several human mutations associated with idiopathic generalized

Table 1. Electrophysiological properties of human $Ca_v3.2$ channel variants expressed in tsA-201 cells. Activation and inactivation kinetic values are shown for a depolarization step to -40 mV from a holding potential of -100 mV.

Ca _v 3.2 variant	Activation				Inactivation				RFI			
	V _{0.5} (mV)	k	τ (ms)	(n)	G _{max} (pS/pF)	(n)	V _{0.5} (mV)	k	τ (ms)	(n)	τ (ms)	(n)
WT	-39.9 ± 0.6	5.6 ± 0.2	5.8 ± 0.2	45	688 ± 59	45	-69.8 ± 0.6	4.4 ± 0.1	21.9 ± 1.0	32	377 ± 35	11
V681L	-43.4 ± 0.9**	5.4 ± 0.2	5.1 ± 0.3	45	756 ± 49	45	-75.3 ± 1.2***	4.4 ± 0.1	18.4 ± 0.9*	30	373 ± 29	18
D1233H	-41.1 ± 0.8	5.0 ± 0.2*	5.8 ± 0.3	48	640 ± 60	48	-70.0 ± 0.7	4.1 ± 0.1	19.3 ± 1.1	34	343 ± 30	15
V681L+D1233H	-40.8 ± 0.6	5.6 ± 0.1	5.7 ± 0.2	30	644 ± 58	30	-74.0 ± 1.0**	4.7 ± 0.2	20.6 ± 0.8	31	435 ± 24	27

epilepsy and located within the I-II loop and II-III-loop of Ca_v3.2 alter channel gating [19–22]. Consistent with these observations, our functional analysis of Ca_v3.2 missense variants revealed several alterations of the gating properties of the channel. For instance, the V681L mutation produced a hyperpolarized shift of the voltage dependence of activation, as well as a concomitant hyperpolarized shift of the voltage dependence of inactivation. From a mechanistic viewpoint, this apparent mix gain- and loss-of-channel function can be explained by a model in which the V681L mutation may destabilize the closed state of the channel. This notion has recently been proposed for Ca_v3.3 channels [23] and is consistent with the observation that T-type channels inactivate from both open and closed states [24,25]. Of particular importance is the observation that as a result of the effect on the voltage-dependence of activation and inactivation, the V681L mutation caused a marked decrease of the window current supported by Ca_v3.2 channel. Likewise, decrease of the window current was also observed with the D1233H as a result of the increased slope of the activation curve without alteration of the mid-voltage.

The question then arises as to how channel defects caused by the V681L and D1233H mutations may contribute to the disease phenotype. Alteration of the window current appears particularly relevant as an underlying mechanism of the amyotrophy observed in the proband for several reasons. First, Ca_v3.2 channels are functionally expressed in embryonic skeletal muscle fibers where they present a developmental expression pattern consistent with a role in early-stage muscle differentiation. For instance, the T-type current density in muscle fibers increases transiently during prenatal myogenesis to reach a maximum expression at embryonic day E16 before to decrease dramatically until birth [26]. Second, extracellular calcium is required for the fusion of myoblasts [27] and a rise in intracellular calcium level precedes fusion [28,29]. Third, it was proposed that rise in intracellular calcium levels occurs via the window current supported by Ca_v3.2 channels in response to the hyperpolarization of the plasma membrane that precedes the fusion of the myoblasts [30]. Therefore, our observation

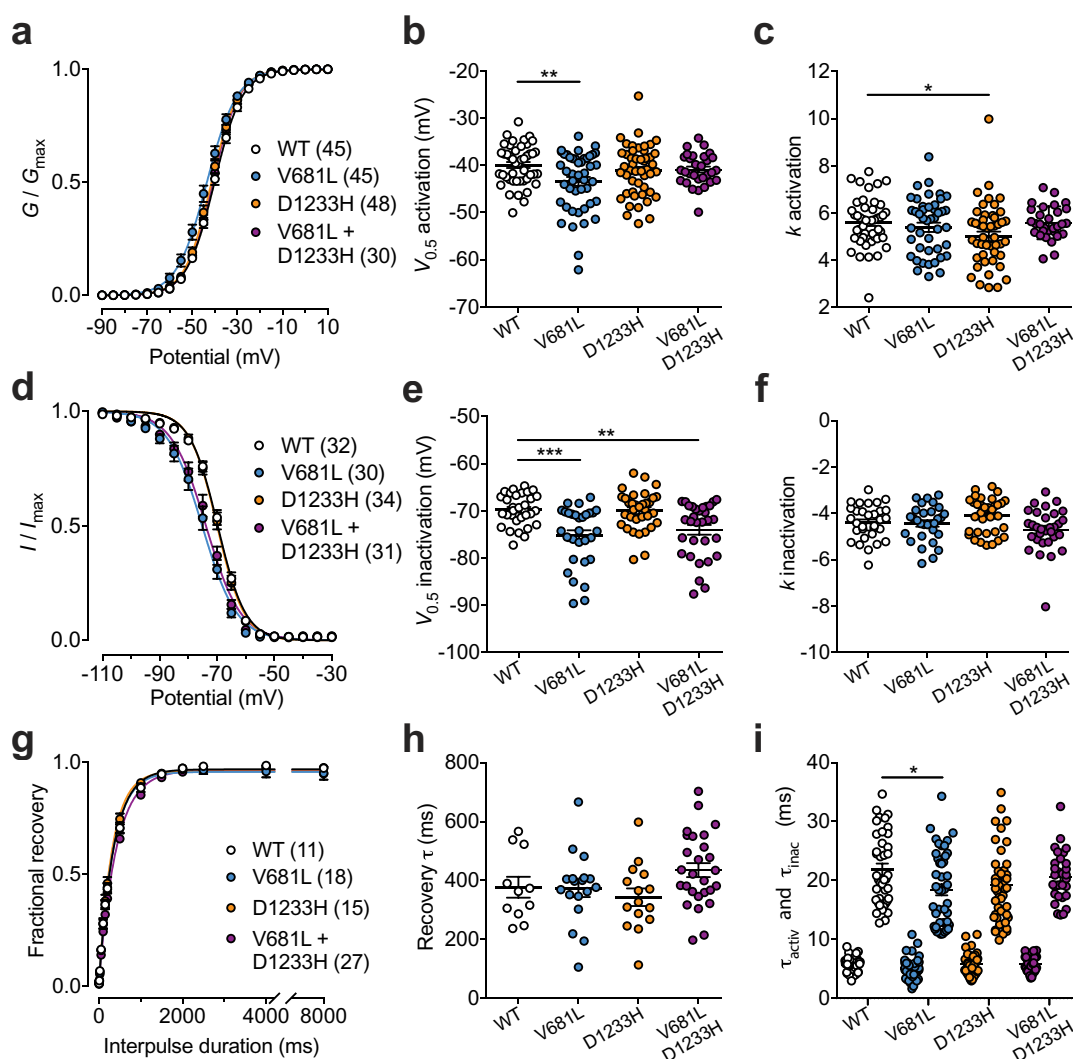


Figure 3. Electrophysiological properties of $Ca_v3.2$ variants. (a) Mean normalized voltage-dependence of T-type current activation for cells expressing WT (white circles), V681L (blue circles), D1233H (orange circles), and co-expressing V681L and D1233H channel variants (purple circles). (b) Corresponding mean half-activation potential values obtained from the fit of the activation curves with the modified Boltzmann Equation (2). (c) Corresponding mean activation slope factor. (d) Mean normalized voltage-dependence of steady-state inactivation. (e) Corresponding mean half-inactivation potential values obtained from the fit of the inactivation curves with the two-state Boltzmann function (3). (f) Corresponding mean inactivation slope factor. (g) Mean normalized recovery from inactivation kinetics. (h) Corresponding mean time constant τ values of recovery from inactivation obtained by fitting recovery curves with the single-exponential function (4). (i) Mean time constant τ values of activation and inactivation of T-type currents obtained by fitting the rising and decay phase of the current with a single exponential function, respectively.

that the p.V681L and p.D1233H mutations caused a reduction of the window current could have an important consequence at early stages of muscle differentiation and may represent an underlying mechanism of infantile-onset amyotrophy (Figure 5(a)). Additionally, several studies have reported the expression of T-type channels in motor neurons [31,32]. Although the role of T-type channels in motor neurons has not been investigated yet, it is likely that they contribute to

some forms of neuronal excitability. Therefore, alteration of T-type channel activity is likely to affect muscle afferent signaling which may participate to some extent to motor symptoms.

In summary, we identified new *CACNA1H* variants in an individual with infantile-onset NMD. Clinical, histopathological, and electrophysiological findings indicating a loss-of- $Ca_v3.2$ channel function suggest that severe congenital amyotrophy may be related to *CACNA1H*, which add to the

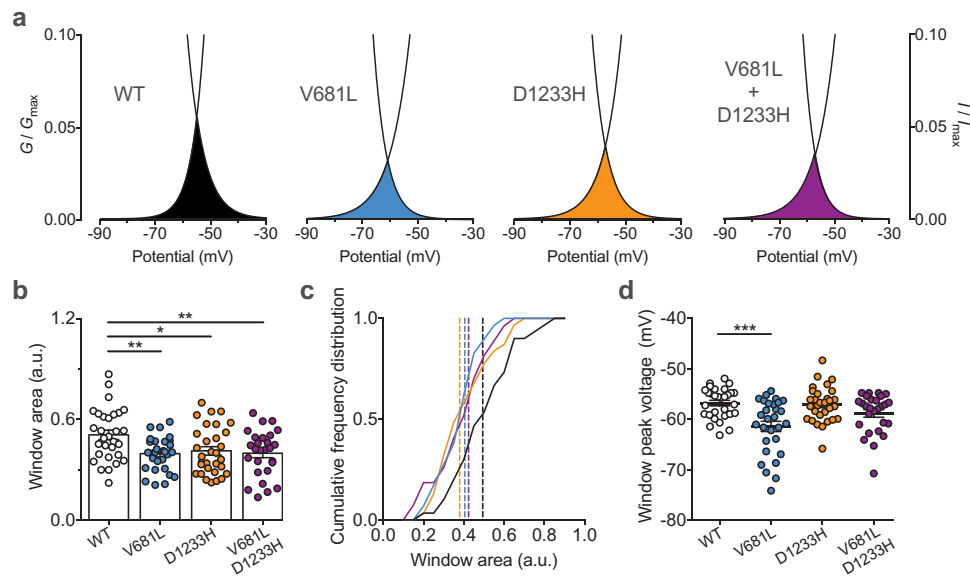


Figure 4. Window current of $Ca_v3.2$ variants. (a) Representative activation (G/G_{max}) – inactivation curves (I/I_{max}) showing the window current for cells expressing WT (black), V681L (blue), D1233H (orange), and co-expressing V681L and D1233H channel variants (purple). (b) Corresponding mean window current measured as the area of the overlap between the activation and inactivation curves. (c) Corresponding frequency plot for each distribution. The dotted lines indicate the median values (WT: 0.4936; V681L: 0.4047; D1233H: 0.3792; V681L + D1233H: 0.4233). (d) Corresponding mean peak-voltage of the window currents. (d) Corresponding mean peak-voltage of the window currents.

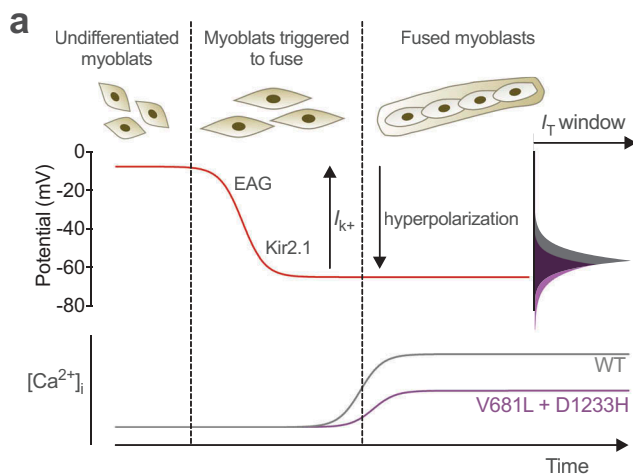


Figure 5. Hypothetical model for altered myogenesis by $Ca_v3.2$ variants. While the membrane potential of undifferentiated myoblast is about -8 mV, sequential expression of the slow-inactivating voltage-gated ether-a-go-go (EAG) and inward-rectifying Kir2.1 potassium channels brings the membrane potential to approximately -65 mV (red line), allowing window calcium influx through $Ca_v3.2$ channels (grey line) required for the fusion of myoblasts. Reduced window current caused by the V681L and D1233H mutations results in a decreased window calcium influx (purple line) which potentially compromises early stage myogenesis. Adapted from [30].

growing list of *CACNA1H* channelopathies and would represent a new phenotype associated with mutations in this gene.

Acknowledgments

We thank family members for participating in this study.

Disclosure statement

The authors report no conflict of interest.

Funding

A.T. is supported by a postdoctoral fellowship from the Institute of Organic Chemistry and Biochemistry (IOCB). N.W. is supported by the IOCB.

ORCID

Melissa T. Carter <http://orcid.org/0000-0001-7211-3731>
 Andriy Tomin <http://orcid.org/0000-0001-8921-6366>
 Norbert Weiss <http://orcid.org/0000-0002-0040-1109>

References

- [1] Zatz M, Passos-Bueno MR, Vainzof M. Neuromuscular disorders: genes, genetic counseling and therapeutic trials. *Genet Mol Biol.* 2016;39(3):339–348.
- [2] Laing NG. Genetics of neuromuscular disorders. *Crit Rev Clin Lab Sci.* 2012;49(2):33–48.

- [3] Lamar KM, McNally EM. Genetic modifiers for neuromuscular diseases. *J Neuromuscul Dis.* 2014;1(1):3–13.
- [4] Steinberg KM, Yu B, Koboldt DC, et al. Exome sequencing of case-unaffected-parents trios reveals recessive and de novo genetic variants in sporadic ALS. *Sci Rep.* 2015;5:9124.
- [5] Rzhpetskyy Y, Lazniewska J, Blesneac I, et al. CACNA1H missense mutations associated with amyotrophic lateral sclerosis alter Cav3.2 T-type calcium channel activity and reticular thalamic neuron firing. *Channels (Austin).* 2016;466–477.
- [6] Weiss N, Zamponi GW. T-type calcium channels: from molecule to therapeutic opportunities. *Int J Biochem Cell Biol.* 2019;108:34–39.
- [7] Perez-Reyes E. Molecular physiology of low-voltage-activated t-type calcium channels. *Physiol Rev.* 2003;83(1):117–161.
- [8] Zamponi GW, Striessnig J, Koschak A, et al. The physiology, pathology, and pharmacology of voltage-gated calcium channels and their future therapeutic potential. *Pharmacol Rev.* 2015;67(4):821–870.
- [9] Gambardella A, Labate A. The role of calcium channel mutations in human epilepsy. *Prog Brain Res.* 2014;213:87–96.
- [10] Splawski I, Yoo DS, Stotz SC, et al. CACNA1H mutations in autism spectrum disorders. *J Biol Chem.* 2006;281(31):22085–22091.
- [11] Lu AT, Dai X, Martinez-Agosto JA, et al. Support for calcium channel gene defects in autism spectrum disorders. *Mol Autism.* 2012;3(1):18.
- [12] Souza IA, Gandini MA, Wan MM, et al. Two heterozygous Cav3.2 channel mutations in a pediatric chronic pain patient: recording condition-dependent biophysical effects. *Pflugers Arch.* 2016;468(4):635–642.
- [13] Scholl UI, Stölting G, Nelson-Williams C, et al. Recurrent gain of function mutation in calcium channel CACNA1H causes early-onset hypertension with primary aldosteronism. *Elife.* 2015;4:e06315.
- [14] Daniil G, Fernandes-Rosa FL, Chemin J, et al. CACNA1H mutations are associated with different forms of primary aldosteronism. *EBioMedicine.* 2016;13:225–236.
- [15] Dubel SJ, Altier C, Chaumont S, et al. Plasma membrane expression of T-type calcium channel alpha(1) subunits is modulated by high voltage-activated auxiliary subunits. *J Biol Chem.* 2004;279(28):29263–29269.
- [16] Proft J, Rzhpetskyy Y, Lazniewska J, et al. The Cacna1h mutation in the GAERS model of absence epilepsy enhances T-type Ca²⁺ currents by altering calnexin-dependent trafficking of Ca_v3.2 channels. *Sci Rep.* 2017;7(1):11513.
- [17] Vitko I, Bidaud I, Arias JM, et al. The I-II loop controls plasma membrane expression and gating of Ca(v)3.2 T-type Ca²⁺ channels: a paradigm for childhood absence epilepsy mutations. *J Neurosci.* 2007;27(2):322–330.
- [18] Arias-Olguín II, Vitko I, Fortuna M, et al. Characterization of the gating brake in the I-II loop of Ca(v)3.2 T-type Ca(2+) channels. *J Biol Chem.* 2008;283(13):8136–8144.
- [19] Khosravani H, Altier C, Simms B, et al. Gating effects of mutations in the Cav3.2 T-type calcium channel associated with childhood absence epilepsy. *J Biol Chem.* 2004;279(11):9681–9684.
- [20] Khosravani H, Bladen C, Parker DB, et al. Effects of Cav3.2 channel mutations linked to idiopathic generalized epilepsy. *Ann Neurol.* 2005;57(5):745–749.
- [21] Peloquin JB, Khosravani H, Barr W, et al. Functional analysis of Ca_v3.2 T-type calcium channel mutations linked to childhood absence epilepsy. *Epilepsia.* 2006;47(3):655–658.
- [22] Eckle VS, Shcheglovitov A, Vitko I, et al. Mechanisms by which a CACNA1H mutation in epilepsy patients increases seizure susceptibility. *J Physiol.* 2014;592(4):795–809.
- [23] Jurkovicova-Tarabova B, Cmarko L, Rehak R, et al. Identification of a molecular gating determinant within the carboxy terminal region of Ca_v3.3 T-type channels. *Mol Brain.* 2019;34.
- [24] Frazier CJ, Serrano JR, George EG, et al. Gating kinetics of the alpha1I T-type calcium channel. *J Gen Physiol.* 2001;12(1):457–470.
- [25] Serrano JR, Perez-Reyes E, Jones SW. State-dependent inactivation of the alpha1G T-type calcium channel. *J Gen Physiol.* 1999;114(2):185–201.
- [26] Berthier C, Monteil A, Lory P, et al. Alpha(1H) mRNA in single skeletal muscle fibres accounts for T-type calcium current transient expression during fetal development in mice. *J Physiol.* 2002;539(3):681–691.
- [27] Wakelam MJ. The fusion of myoblasts. *Biochem J.* 1985;228(1):1–12.
- [28] Entwistle A, Zalin RJ, Bevan S, et al. The control of chick myoblast fusion by ion channels operated by prostaglandins and acetylcholine. *J Cell Biol.* 1988;106(5):1693–1702.
- [29] Rapuano M, Ross AF, Prives J. Opposing effects of calcium entry and phorbol esters on fusion of chick muscle cells. *Dev Biol.* 1989;134(2):271–278.
- [30] Bijlenga P, Liu JH, Espinos E, et al. T-type alpha 1H Ca²⁺ channels are involved in Ca²⁺ signaling during terminal differentiation (fusion) of human myoblasts. *Proc Natl Acad Sci U S A.* 2000;97(13):7627–7632.
- [31] Canto-Bustos M, Loeza-Alcocer E, González-Ramírez R, et al. Functional expression of T-type Ca²⁺ channels in spinal motoneurons of the adult turtle. *PLoS One.* 2014;9(9):e108187.
- [32] Zhang Z, David G. Stimulation-induced Ca(2+) influx at nodes of Ranvier in mouse peripheral motor axons. *J Physiol.* 2016;594(1):39–57.